Journal of Molecular Catalysis A: Chemical 339 (2011) 1–7

Contents lists available at ScienceDirect

Journal of Molecular Catalysis A: Chemical

journal homepage: www.elsevier.com/locate/molcata

Editor's Choice paper

# Cathodic Fenton degradation of 4,6-dinitro-o-cresol with nano-magnetite

Xia Zeng[a], Khalil Hanna[b], Ann T. Lemley[a,*]

[a] Graduate Field of Environmental Toxicology, FSAD, MVR Hall, Cornell University, Ithaca, NY 14853-4401, United States
[b] Laboratoire de Chimie Physique et Microbiologie pour l'Environnement, LCPME, UMR 7564 CNRS-Université Henri Poincaré, 405 rue de Vandoeuvre, 54600 Villers-les-Nancy, France

ARTICLE INFO

*Article history:*
Received 26 January 2011
Received in revised form 1 March 2011
Accepted 3 March 2011

*Keywords:*
Nano-magnetite
DNOC
Cathodic Fenton degradation
Kinetic model

ABSTRACT

The successful removal of 4,6-dinitro-o-cresol (DNOC) is reported using nano-magnetite ($Fe_3O_4$) as the iron source and cathodic Fenton generation of hydrogen peroxide. Operating conditions were optimized by varying the electrolyte concentration, electric current, and $O_2$ flow. The effects of different DNOC initial concentrations, pH values and nano-magnetite quantities on the degradation rate of DNOC were also examined. The results showed that a lower DNOC initial concentration and a lower pH led to faster degradation of DNOC. It was also observed that the amount of nano-magnetite affected the degradation rate at lower pH while having no influence at neutral pH. Both homogeneous and heterogeneous reactions in the system were investigated. The homogeneous reaction dominated at a lower pH; direct electrolysis appears to take place at neutral pH; and a contribution from a heterogeneous reaction was not obvious under the experimental conditions studied. A model was developed to describe the degradation mechanism at low pH conditions, and the model matched experimental data very well. The combination of nano-magnetite and cathodic Fenton provides a fast way to degrade organic contaminants with readily available materials. Furthermore, magnetite is more stable, reusable and easy to separate compared to ferrous salt and other iron rich minerals.



## 1. Introduction

The Fenton reaction has been widely used in the successful remediation of environmental pollutants, especially pesticides [1–4]. Fenton treatment uses a metal catalyst to generate hydroxyl radicals from hydrogen peroxide, and various methods have been used to deliver the catalyst into the reaction system. Anodic Fenton treatment (AFT) was developed to provide a constant delivery of ferrous ion from a sacrificial iron electrode by electrolysis while simultaneously pumping hydrogen peroxide into the system [5,6]. Cathodic Fenton, which generates hydrogen peroxide on a cathode in an electrolytic cell as shown below,

$$O_2 + 2H^+ + 2e^- \rightarrow H_2O_2 \quad (1)$$

was developed to eliminate the need for the direct input of hydrogen peroxide [7–12]. The characteristics and main applications of electro-Fenton have been previously reported by Brillas et al. [13]. Most of the cathodic Fenton processes have been performed in a combined cell where the anode and cathode are placed in an undivided container [7,9–12]. Compared to a split cell, the pH in a combined cell remains constant, and the need for a membrane or bridge is eliminated; therefore, low cell voltage is needed for electrolysis [13]. Furthermore, in the combined cell, oxygen produced at the anode can also help with the generation of hydrogen peroxide on the cathode [8].

Recently, iron oxide minerals, especially magnetite, have been used to replace iron salts in Fenton or Fenton-like reactions [14–17]. Magnetite ($Fe^{II}$–$Fe^{III}$ mixed oxide) was successfully used as an iron source in heterogeneous Fenton reactions, because $Fe^{II}$ plays an important role in the initiation of the Fenton reaction according to the classical Haber–Weiss mechanism [16]. Magnetite was shown to catalyze the oxidative degradation of target compounds effectively, and it exhibited good structural stability and excellent reusability [17,18]. When magnetite is used as an iron source, both heterogeneous Fenton and homogeneous Fenton reactions may occur. Some chemical conditions such as acidic pH and/or use of a chelating agent can improve the leaching of iron from the solid surface, thus propagating the homogeneous reaction with the dissolved iron and thereby contributing to improvement in the oxidation efficiency [17].

Previous work has reported the decomposition of aniline by combining magnetite (5 μm powder) and the cathodic Fenton process [19] achieving 60% removal of pollutant after 5 h of mineralization. To achieve a faster decomposition rate of pollutant, nanoparticles of magnetite can provide a large exposed surface area in the reaction medium and thus improve the favorability of both heterogeneous and homogeneous reactions. Indeed, this large reactive surface may expedite both the surface interactions

* Corresponding author. Tel.: +1 607 255 3151; fax: +1 607 255 1093.
*E-mail address:* ATL2@cornell.edu (A.T. Lemley).

1381-1169/$ – see front matter © 2011 Elsevier B.V. All rights reserved.
doi:10.1016/j.molcata.2011.03.001

and the dissolution of iron, making nano-magnetite an attractive alternative to micrometer-size magnetite.

In the present study we explored the feasibility of combining nano-magnetite and cathodically produced hydrogen peroxide in the degradation of 4,6-dinitro-o-cresol (DNOC), a pesticide previously widely used. DNOC was banned by the US-EPA due to its long term health effects on humans [20] but is still found in large amounts in the environment due to its slow degradation rate [21,22]. The destruction of DNOC was previously reported using the cathodic Fenton method and ferric salt as an iron source [23].

It is important to understand the reaction mechanisms for a combined Fenton system of nano-magnetite and cathodically generated $H_2O_2$ in order to optimize the degradation of target compounds. Possible reactions include: a homogeneous Fenton reaction in the solution, a heterogeneous Fenton reaction occurring on the active sites of the magnetite surface, and direct electrolysis. The objectives of this work were to: (i) optimize the operating conditions of cathodic Fenton treatment with nano-magnetite; (ii) investigate the possible degradation reactions occurring in the cell under different conditions; and (iii) develop a kinetic model for cathodic Fenton treatment of DNOC using nano-magnetite.

## 2. Experimental

### 2.1. Chemicals

Sodium sulfate, sodium acetate, ferric sulfate 7-hydrate, acetic acid, hydroxylamine hydrochloride, 1,10-phenanthroline, methanol (HPLC grade), water (HPLC grade) and acetronitrile (HPLC grade) were purchased from Fisher Scientific (Fair Lawn, NY). Ferrous sulfate 7-hydrate and hydrogen peroxide (30%) were purchased from Mallinckrodt (Paris, KY). Iron standard solution (10 mg/L) was purchased from HACH (Loveland, CO). DNOC was purchased from Chem Service (West Chester, PA). DI water was obtained from an MP-1 Mega-Pure™ system (Corning, NY) with electric resistance greater than 18.1 MΩ/cm. All commercial chemicals were used directly without further purification/treatment.

### 2.2. Solid characterization

The nano-magnetite sample was purchased from Nanostructured & Amorphous Materials Inc. (Houston, TX). In order to identify the crystal structure of the mineral, a sample of solid was analyzed by X-ray powder diffraction (XRD). The XRD data were collected with a D8 Bruker diffractometer, equipped with a monochromator and a position-sensitive detector. The X-ray source was a Co anode ($\lambda = 0.17902$ nm). The diffractogram was recorded in the 3–64° $2\theta$ range, with a 0.0359° step size, and a collecting time of 3 s per point. Scanning Electron Microscopy (SEM) displayed the morphology of the iron oxide. The SEM images were collected with a HITACHI FEG 54800 apparatus, and the SEM microscope was generally operated with a beam current of 3 pA and an accelerating voltage of 20 kV (analyzed microvolume of $\sim 6\ \mu m^3$). The solid powder was glued on an adhesive surface and metalized with a thin layer of gold. Transmission Electron Microscopy (TEM) analysis provides information regarding morphology (the size, shape and arrangement of the particles) and structural and compositional data (on areas a few nanometers in diameter). TEM observations were carried out with a Philips CM20 TEM (200 kV) coupled with an EDAX energy dispersive X-ray spectrometer. The solid powder was re-suspended in 2 mL ethanol under ultrasonication, and a drop of suspension was evaporated on a carbon-coated copper grid which was placed on filter paper. A spot size of about 70 nm and a counting time of 40 s were used to record the EDX spectra. EDX calibration standards were run to obtain quantitative analyses of major and trace elements with a detection limit of approximately 100 ppm.

The specific surface area of the iron oxide was determined by multipoint $N_2$-BET analysis using a Coulter (SA 3100) surface area analyzer. Potentiometric titrations of the oxide were conducted in a thermostated double walled pyrex cell at 293 K in 0.001, 0.01 and 0.1 M NaCl solutions. The $N_2$ gas was constantly passed through the suspensions to bubble out the $CO_2$. The pH value of the suspension was adjusted with titrant solutions (HCl or NaOH). The blank titrations were also performed with similar solutions in the absence of the solid. In addition, the electrophoretic mobility of the particles was measured with a Malvern Zetasizer (NanoZS) as a function of pH in 10 mM NaCl solution and the zeta potential was calculated from the electrophoretic mobility. The iso-electric point (7.8) of iron oxides are in agreement with the point of zero charge (PZC) determined by potentiometric titration (7.6) and close to the values reported in the literature [17,18].

### 2.3. Adsorption of DNOC to nano-magnetite

In order to determine time to adsorption equilibrium, 1 g of nano-magnetite was stirred with 200 mL of 11.4 μg/mL DNOC solution for 3 h. Based on the results, degradation experiments were performed with DNOC solutions that had been stirred with nano-magnetite for 3 h. For the sorption isotherm test, 15 mL solutions with a range of DNOC concentrations were shaken with 0.12 g nano-magnetite in a 50 mL tube for 3 h. The solutions were then centrifuged and decanted. The DNOC concentrations in the supernatants were measured by HPLC.

### 2.4. Degradation of DNOC

Fenton experiments were carried out in a 400 mL undivided cylindrical cell containing a graphite cathode and anode. The graphite electrode is stable and exhibits a high overpotential for $H_2$ evolution and low activity for $H_2O_2$ decomposition [13]. Typically, 200 mL of 11.4 μg/mL DNOC solution with 1 g nano-magnetite was added to the cell, and $Na_2SO_4$ was added into the solution as an electrolyte. After optimization, 0.08 M $Na_2SO_4$, 0.025A of current and 40 mL/min of $O_2$ flow were used to degrade the target compound. An aliquot of 1.0 mL solution was taken out at specific time intervals and 0.1 mL methanol was added to quench the hydroxyl radical. The sample was then centrifuged for 10 min and the supernatant was analyzed by HPLC. Each experiment was repeated twice.

$H_2SO_4$ was used to adjust the initial pH in solution. The pH was measured using an Accumet Basic AB15 pH meter (Fisher Scientific). When simulating the $H_2O_2$ generated on the cathode at neutral pH, 5.8 mM $H_2O_2$ solution was pumped into the system at a constant delivery rate of 0.5 mL/min.

### 2.5. Measurement of DNOC concentration

The concentration of DNOC was measured by an Agilent 1100 HPLC with a DAD detector (Agilent Technologies, Inc., Santa Clara, CA). The mobile phase was composed of 80% methanol and 20% water (pH was adjusted to 3 by phosphoric acid). A C-18 5 μm 250 mm × 4.6 mm (i.d.) Restek reverse phase column was used. Flow rate, injection volume and column temperature were set to 1.0 mL/min, 20 μL and 25 °C, respectively. The UV wavelength for the DAD was set at 269 nm. Calibration of the instrument was performed using a series of DNOC solutions, and the calibration curve indicated that peak area in HPLC was directly proportional to the concentration of DNOC. Therefore the data of relative peak areas were used to represent DNOC concentrations in this study.

### 2.6. Measurement of $H_2O_2$ and iron concentration in solution

The concentration of $H_2O_2$ generated on the cathode was measured by the iodide method [24] and analyzed by a Lambda 35 UV/VIS spectrometer (PerkinElmer Instruments, Waltham, MA) at 352 nm. Ferrous and total iron concentration in solution were measured by 1,10-phenanthroline according to the Standard Method for the Examination of Water and Wastewater [25] and analyzed by a UV/VIS spectrometer at 510 nm.

### 2.7. Experimental data analysis

The model fitting and statistical analyses were performed using Sigmaplot 9.01 (Systat Software Inc., Richmond, CA).

## 3. Results and discussion

### 3.1. Nano-magnetite characterization

The XRD diffractogram of the solid powder is shown in Fig. S-1A. Five observed diffraction peaks at $2\theta = 21.2^\circ$, $35^\circ$, $41.2^\circ$, $50.4^\circ$ and $62.8^\circ$ can be assigned to $Fe_3O_4$ magnetite [26]. The *d*-space values of these main peaks are 2.53, 2.96, 2.09, 4.85 and 1.71 Å, which may correspond to the more intense lines 311, 220, 400, 111 and 422, respectively, of magnetite. Bragg peaks of the smaller particles exhibit peak broadening as expected for nanoparticles [26]. Magnetite ($Fe_3O_4$) is usually represented by the formula $(Fe^{3+})_{tet}[Fe^{3+}Fe^{2+}]_{oct}O_4$ [17,26]. Magnetite ($Fe_3O_4$) has an inverse spinel structure in which cations occupy tetrahedral and octahedral sites in the face-centered cubic close-packed oxygen lattice.

The typical SEM image shows that the nano-magnetite particles are quasi-spherical and highly aggregated (Fig. S-1B). The average size of the particles is ~30 nm. The specific surface area (SSA) experimental value of magnetite determined by the BET method was found to be $48 \pm 2\ m^2/g$. The radius of the spherical particles (the density of magnetite, $\rho = 5.15 \times 10^6\ g/m^3$) can be related to the surface area as $A = 6/(\rho d) = 48\ m^2/g$. Thus, the calculated average diameter of a supposed spherical particle is ~25 nm, which is consistent with the average size estimated by the SEM observations.

The XRD diffractogram recorded at the end of the oxidation reaction was found to be similar to that recorded before the reaction, indicating the structural stability of nano-magnetite during the cathodic Fenton treatment (data not shown).

TEM images of the nano-magnetite sample revealed the agglomeration of small spherical particles of magnetite of ~30 nm (Fig. S-1C). Electron diffraction patterns provided by TEM can also be used to characterize the crystal structure of particles. Transmission Electron Microscopy (TEM) combined with energy-dispersive X-ray spectrometry (EDXS) yields an elemental analysis of sample. Elemental ratios can be calculated by EDXS and compared with known mineralogical composition. EDX microanalyses of sample before and after oxidation reaction showed the characteristic Fe/O ratio of magnetite ($Fe_3O_4$).

### 3.2. DNOC sorption test

The sorption of DNOC on nano-magnetite at pH 2.8 is shown in Fig. S-2. The results indicate that ~20% of DNOC was adsorbed to nano-magnetite after 3 h and that the sorption reached equilibrium after 2 h. Before measuring the cathodic Fenton degradation of DNOC in the current work, nano-magnetite was stirred with the DNOC solution for 3 h to ensure that the sorption had reached equilibrium, at which point the sorption isotherm was measured (Fig. S-3). The sorbed amount at pH 2.8, determined at 22 mg/mL DNOC, is equivalent to 7.6 μmol/g or 0.16 μmol/m$^2$, too low comparable to the density of reactive sites on iron oxides (2.31 sites/nm$^2$ or 3.8 μmol/m$^2$) to saturate them [26].

In the lower concentration range, DNOC showed similar sorption affinity for both pH values 2.8 and 5.9 (Fig. S-3). In previous work, the adsorption envelope of ionizable compounds such as DNOC on iron oxides has typically shown maximum adsorption at a pH near the p$K_a$ [27]. Since DNOC is a weak acid (p$K_a$ = 4.4) [28], maximum sorption can be obtained in the pH range of 4.4–7.6 (pzc value of magnetite), where the DNOC is negatively charged and iron oxide particles are positively charged. In the current work the charge repulsion was expected at lower (<4.4) or higher (>7.6) pH values where the sorbate and sorbent were both positively or negatively charged. At the high concentration range of sorbate, the adsorption at acidic pH is, however, slightly higher than at pH 5.9 (Fig. S-3). This discrepancy is probably due to non-specific interactions such as hydrophobic and/or Vander Waals forces, which may occur for the sorption of hydrophobic compounds onto iron oxides at a high sorbate loading [29].

### 3.3. Optimization of experimental conditions

A 0.08 M concentration of $Na_2SO_4$ proved to be the most efficient for producing $H_2O_2$ when compared with 0.04 M and 0.16 M (Table S-1). Electric current was supplied and set at 0.025A by a BK Precision DC power supply 1610. Higher current required greater voltage and caused other side reactions, resulting in slower degradation of the target compound. An $O_2$ flow at 40 mL/min was determined most efficient to generate $H_2O_2$ and a higher flow rate did not improve the reaction.

### 3.4. Degradation of DNOC

Degradation of DNOC was performed with different initial concentrations, and the results are shown in original and logarithmic format in Fig. S-4. The degradation rate was first order and decreased with increasing initial concentration. The process may involve competition between the byproducts and DNOC for the hydroxyl radical which has been reported previously by others [10,11]. Although there may be small byproducts of DNOC degradation, the detection of them is not possible by HPLC or mass spectrometry due to their instability and ionic form [28,30]. Therefore, the degradation pathway and byproducts of DNOC were not studied in this current work.

In a heterogeneous system the decrease of the first-order degradation rate constant with an increase in the initial concentration of the pollutant may reflect a competition between the pollutant and oxidant toward the magnetite surface. The increased amount of pollutant may occupy a greater number of iron active sites which become unavailable for $H_2O_2$ and result in a lower HO· generation rate. More pollutant sorbs on the magnetite surface and less $H_2O_2$ interacts with the iron surface and thus less hydroxyl radical is formed at the surface [18]. The Langmuir–Hinshelwood model postulates that the rate of reaction of two species adsorbed on the surface is the rate-limiting step [18]:

$$\frac{1}{k_{app}} = \frac{1}{k_{int}} \cdot [DNOC]_i + \frac{1}{k_{int} K_s}, \quad (2)$$

where $k_{app}$ is the initial pseudo-first-order rate constant (min$^{-1}$), $k_{int}$ is the intrinsic reaction rate constant (mg L$^{-1}$ min$^{-1}$), and $K_s$ is the adsorption constant of DNOC on the magnetite surface (L mg$^{-1}$).

To test the validity of this model for DNOC degradation in this system, the pseudo-first-order rate constant was determined at different initial DNOC concentrations and its reciprocal ($1/k_{app}$) was plotted against the initial concentration of DNOC. The calculated values of $k_{int}$ and $K_s$ are 0.43 mg L$^{-1}$ min$^{-1}$ and 0.73 L mg$^{-1}$, respectively, and as shown in Fig. S-5 the linear correlation ($R^2$)

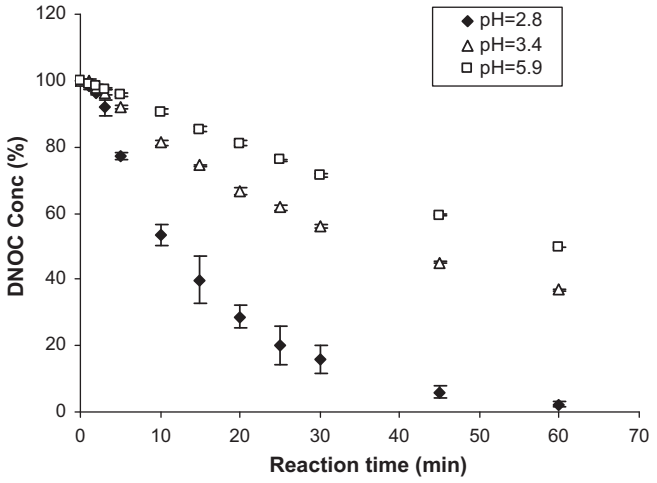


**Fig. 1.** DNOC degradation at different initial pH values (initial [DNOC] = 11.4 μg/mL).

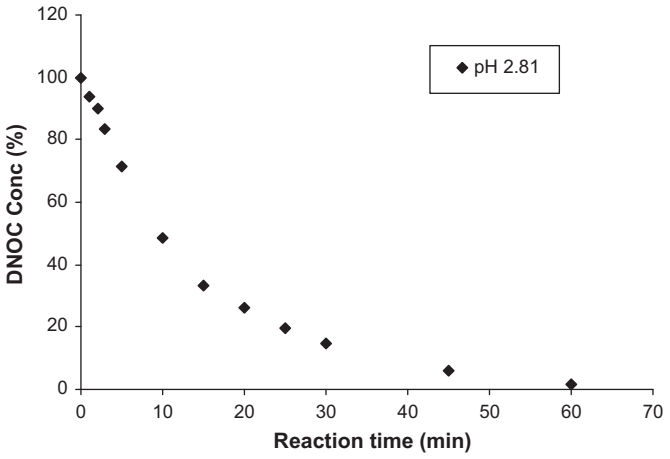


**Fig. 3.** Degradation of DNOC with 4.14 μg/mL $Fe^{2+}$ and 1.76 μg/mL $Fe^{3+}$ at pH 2.8. The initial concentration of DNOC and the current are 11.4 μg/mL and 0.025 A, respectively. No magnetite was added.

between $1/k_{app}$ and $[DNOC]_i$ is 0.95. The low value of $R^2$ does not allow a prediction of the probability for a heterogeneous reaction in this system.

The degradation of DNOC at different pHs and nano-magnetite quantities was investigated in order to determine the contribution of homogeneous and heterogeneous Fenton reactions and other possible reactions under different conditions. The hydrogen peroxide and total iron ion concentrations during the reaction were measured, and control tests were performed by adding the same amount of iron or hydrogen peroxide as measured during the reaction of cathodic Fenton with nano-magnetite. A chelating agent was also used at neutral pH conditions to determine the contribution of homogeneous versus heterogeneous Fenton and other possible surface reactions.

The results of DNOC degradation at three different pH values (2.8, 3.4 and 5.9) show that lower pH expedited the reaction (Fig. 1). The faster degradation of DNOC at lower pH may be caused by a higher concentration of iron released into the solution and/or by more hydrogen peroxide generated on the cathode. To explore the dissolution of iron ion from nano-magnetite particles, ferrous ion and total iron were measured during the cathodic Fenton reaction (Fig. 2). Although $Fe^{3+}$ can be reduced to $Fe^{2+}$ on the graphite cathode according to a previous study [13], the ratio of $Fe^{3+}$:$Fe^{2+}$ increased with reaction time, suggesting that the oxidation of $Fe^{2+}$ by $H_2O_2$ generated on the cathode was the major reaction during the Fenton reaction. The concentration of ferrous ion was highest at lowest pH (2.8), causing the fastest degradation of DNOC. At pH 5.9, iron concentration was below the detection limit; however, the concentration of DNOC decreased to about half of its initial concentration, suggesting that degradation of DNOC at neutral pH was not caused by the homogeneous Fenton reaction in the solution. While the degradation of DNOC at neutral pH can be caused by a heterogeneous reaction on the nano-magnetite surface, it has also been reported that pesticides can be degraded by direct electrolysis during electro-Fenton treatment [31]. Therefore, direct electrolysis of DNOC was also investigated as a degradation path for DNOC at neutral pH.

To determine whether the homogeneous Fenton reaction was the only reaction under acidic conditions, the same amount of $Fe^{2+}$ and $Fe^{3+}$ salts as measured in 1 g magnetite dissolved at pH 2.8 (as shown in Fig. 2A) was used as a Fenton control test and the results are shown in Fig. 3. The degradation rate of DNOC in the control test was found to be very close to that in the degradation with magnetite at pH 2.8 (Fig. 1). This result implies that dissolved iron ion was mainly responsible for the Fenton degradation of DNOC, and that homogeneous Fenton degradation is the primary reaction occurring in the solution under acidic conditions.

This tentative conclusion for the reaction under acidic conditions can also be tested by running a control test for the generation of $H_2O_2$ at the cathode. The concentration of $H_2O_2$ was measured

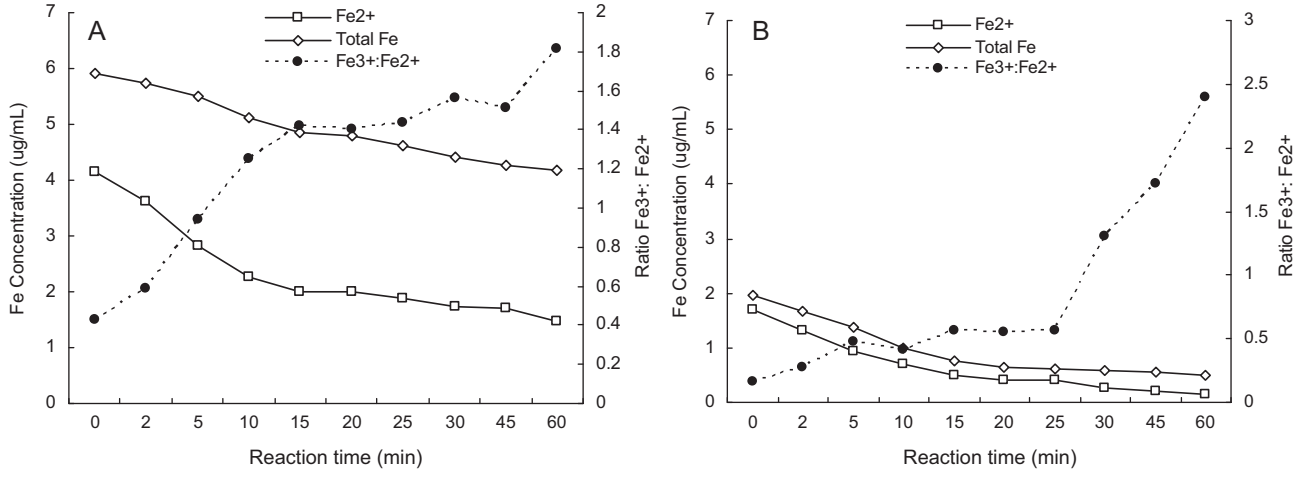


**Fig. 2.** Ferrous and total iron ion concentration during cathodic Fenton degradation of DNOC at different pHs (A = 2.8, B = 3.4). No iron ion was detected in solution at pH 5.9 (initial [DNOC] = 11.4 μg/mL).

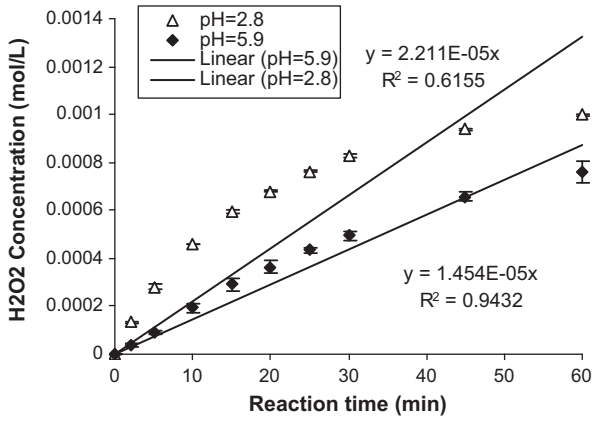


**Fig. 4.** Concentration of $H_2O_2$ generated at the cathode at two different pH values.

at two different pH conditions (2.8 and 5.9) and is shown in Fig. 4. The generation rate of $H_2O_2$ was higher at lower pH, and in both cases, the concentration of $H_2O_2$ increased linearly in the first few minutes and tended to reach a plateau after 60 min. As reported by others, the accumulated $H_2O_2$ can be destroyed on the anode in an undivided cell, leading to a quasi-steady state value after a few hours of electrolysis [13].

In order to simulate the generation rate of $H_2O_2$ concentration over time, the assumption was made that $H_2O_2$ is generated linearly (Fig. 4), and this amount of $H_2O_2$ was pumped into the system for the control experiments. The degradation results from these control experiments are compared with those from experiments with $H_2O_2$ generated at the cathode in Fig. 5. The degradation rate of DNOC with pumped in $H_2O_2$ was found to be very close to that with cathodic Fenton at pH 2.8 (Fig. 5A). This result implies that at acidic pH (2.8), the homogeneous Fenton reaction occurring in the solution is the only degradation process. At pH 5.9 the degradation rate of DNOC with pumped in $H_2O_2$ was found to be much lower than that with cathodic Fenton (Fig. 5B), indicating another major source of degradation, most probably the direct destruction of DNOC by electrolysis on the electrode.

Thus, the homogeneous Fenton reaction and direct electrolysis were determined to be the major processes at acidic and near neutral pH, respectively. However, the contribution of heterogeneous Fenton reaction was still not clear. To determine whether a heterogeneous Fenton reaction contributed to the degradation of DNOC, a series of cathodic Fenton treatments of DNOC with different amounts of nano-magnetite were performed at two different pH conditions (Fig. 6). The degradation rate of DNOC decreased with a decreasing amount of nano-magnetite at pH 2.8, indicating that the amount of nano-magnetite affects the dissolution of iron in the solution, which would be expected if a homogeneous reaction is primarily responsible for the degradation of DNOC at pH 2.8. There are two reasons that would suggest that the heterogeneous Fenton reaction is insignificant under acidic conditions. First, the rate of the heterogeneous reaction is directly correlated to the surface area, as well as the amount of the nano-magnetite, but a significant change in the amount of nano-magnetite (from 1 g to 0.05 g) resulted in almost no change in the degradation rate (Fig. 6B). Second, the degradation rate with 1 g of nano-magnetite is very close to that with 4.14 μg/mL $Fe^{2+}$ and 1.76 μg/mL $Fe^{3+}$ at pH 2.8 (Fig. 3), implying that the homogeneous Fenton reaction, rather than the heterogeneous Fenton reaction, is the major reaction at pH 2.8. It was also observed that when there was no $H_2O_2$ (no $O_2$ flow) or when there was no nano-magnetite present in solution (Fig. 6A), the degradation rate did not go to zero. This is most probably due to direct electrolysis of DNOC due to the lack of competition from the Fenton reaction.

At near neutral pH (5.9), the degradation of DNOC was the same for reactions with different amounts of nano-magnetite, with or without $H_2O_2$ ($O_2$ flow) (Fig. 6B). This is strong evidence that the heterogeneous reaction was not occurring in the current system. The variation of nano-magnetite amount affects the amount of exposed surface area or reactive sites per unit volume and should change the degradation rate of DNOC if the heterogeneous reaction occurs. It can be concluded that at the neutral pH (5.9), direct electrolysis of DNOC on the electrode is the main identified reaction for degradation of DNOC. In addition, the degradation rate of DNOC at pH 5.9 increased with higher electric current (Fig. S-6). This further confirmed that direct electrolysis was the main reaction at neutral pH. However, a fourfold increase in current produces only a slight increase in the degradation rate, suggesting a decreased current efficiency which can be attributed to a more active competition of the oxidation of $H_2O_2$ on the anode at a high current intensity. The potential for heterogeneous reactions in this system should be further investigated in future work with more highly adsorbing chemical probes and with nano-magnetite with varying particle sizes and surface areas.

Chelating agents have been reported to facilitate the dissolution of iron at near neutral pH, thus affecting the Fenton process [17]. They were used in this study to further confirm the possible reactions in this Fenton system. Two different chelating agents (EDTA and oxalate) were applied to the system at pH 5.9 and both were found to decrease the degradation of DNOC (Fig. S-7). Generally, chelating agents help to dissolve ferrous ion in the solution (this can happen at both pH values) thus propagating the homogeneous reaction and contributing to the improvement of the total oxidation rate. The negative effect observed may be caused by one of two effects: (i) these ligand compounds act as $HO^{\cdot}$ scavengers by competing actively with DNOC for the reaction with the hydroxyl radical or (ii) they compete with DNOC for direct electrolysis.

In the first case, the reaction rate of EDTA with the hydroxyl radical is $4.0 \times 10^8$ L mol$^{-1}$ s$^{-1}$ at pH = 4.0 and $2.0 \times 10^9$ L mol$^{-1}$ s$^{-1}$ at pH = 9.0, while the reaction rate of the oxalate with the hydroxyl radical is $1.4 \times 10^6$ L mol$^{-1}$ s$^{-1}$. Therefore, EDTA and oxalate can easily be oxidized by hydroxyl radicals and act as $^{\bullet}OH$ scavengers in the Fenton reaction at neutral pH [17,32,33]. On the other hand, the electrolysis of ligands such as EDTA or oxalate has been observed in many remediation studies and therefore competition with DNOC for electrolysis is highly likely [34,35]. These results are not consistent with previous work where EDTA and oxalate dissolved magnetite at neutral pH and increased the overall Fenton oxidation rate [17]. This positive effect on oxidation appears to be offset by the competition effects discussed above.

### 3.5. Model development for DNOC degradation

The degradation of DNOC at neutral pH can be described as a zero order reaction (Fig. 7 $R^2 = 0.9931$) and it only varies with the electric current (Fig. S-6). The zero order degradation rate constant at 0.025 A current is measured as $9.90 \times 10^{-2}$ μg mL$^{-1}$ min$^{-1}$. However, the reaction at acidic pH (2.8) seems to fit a first order mechanism, but not very well at the beginning of reaction. To better describe the kinetics of DNOC degradation, especially in the first few minutes of the reaction, a new fitting model for pH 2.8 was developed, based on a homogeneous reaction in solution. The reduction of $Fe^{3+}$ to $Fe^{2+}$ on the cathode is not a major reaction as discussed in Section 3.4. Therefore, we assume that $Fe^{2+}$ is only consumed by the Fenton reaction to generate $^{\bullet}OH$ and that the total iron concentration in solution is kept constant. The instantaneous concentration of $Fe^{2+}$ will be:

$$[Fe^{2+}] = m - [^{\bullet}OH], \quad (3)$$

where $m$ (μg mL$^{-1}$) is the initial concentration of $Fe^{2+}$.

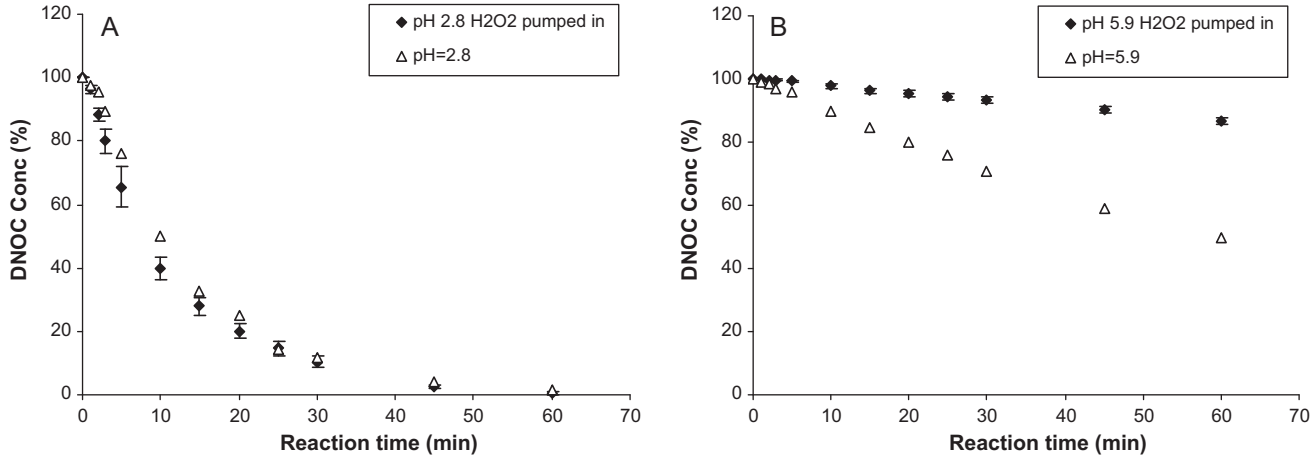


**Fig. 5.** Comparison of DNOC degradation with cathodically generated $H_2O_2$ and pumped in $H_2O_2$ at pH 2.8 (A) and 5.9 (B) (initial [DNOC] = 11.4 μg/mL).

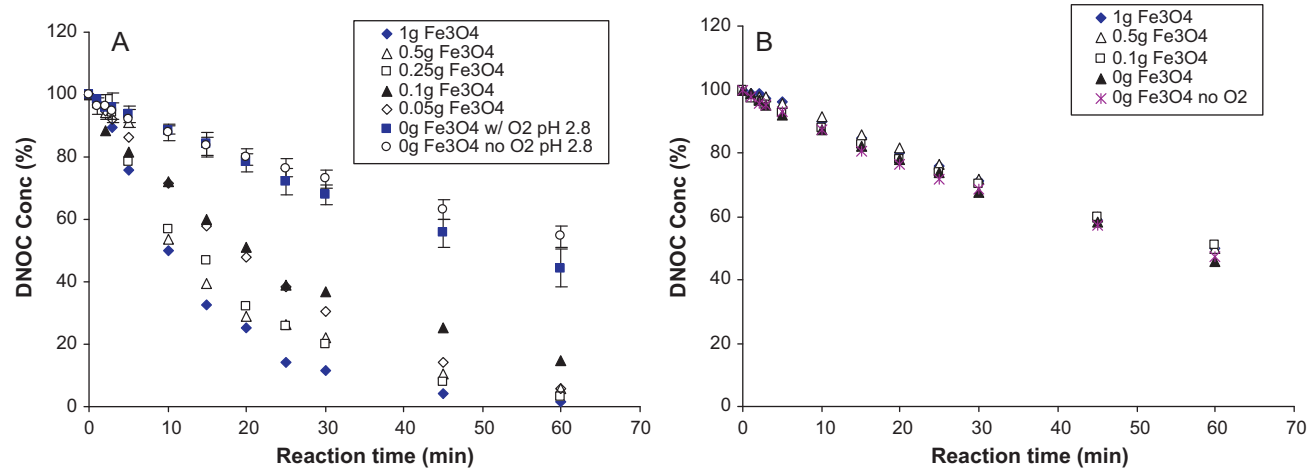


**Fig. 6.** DNOC degradation with different amounts of nano-magnetite at two different pH values (A pH = 2.8, B pH = 5.9, initial [DNOC] = 11.4 μg/mL).

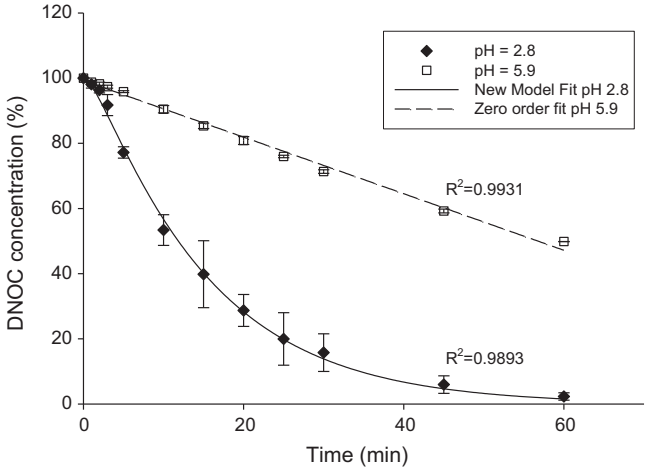


**Fig. 7.** Model fitting of DNOC degradation at different pH values (pH = 2.8 and 5.9).

Because most of the reaction occurred during the first 30 min, we assumed $H_2O_2$ to be generated linearly over time, and the concentration of $H_2O_2$ in solution can be described as:

$$[H_2O_2] = v_0 t, \tag{4}$$

where $v_0$ (μg mL$^{-1}$ min$^{-1}$) is the generation rate and $t$ (min) is the reaction time. Because of the complicated reactions in the reaction system, the $H_2O_2$ generation rate ($v_0$) can be modeled as the cathodic generation rate of $H_2O_2$ by $O_2$ less the rate of $H_2O_2$ destruction on the anode. Although hydroxyl radical is constantly consumed in the reaction, it is very reactive and the rate constant for the hydroxyl radical reaction is much greater than the Fenton reaction. Thus, the Fenton reaction is the controlling step and the instantaneous concentration of hydroxyl radical is proportional to its generation rate [6]:

$$[^{\bullet}OH] = \lambda \left( \frac{d[^{\bullet}OH]}{dt} \right), \tag{5}$$

where λ (min) is the average life of the hydroxyl radical, and the generation rate of the hydroxyl radical is

$$\left( \frac{d[^{\bullet}OH]}{dt} \right) = k_1 [Fe^{2+}][H_2O_2], \tag{6}$$

where $k_1$ is a second-order reaction rate constant (μg$^{-1}$ mL min$^{-1}$) for the generation of hydroxyl radical from Fenton reaction.

Substituting Eqs. (3)–(5) into Eq. (6), we get:

$$[^{\bullet}OH] = k_1 v_0 \lambda t (m - [^{\bullet}OH]). \tag{7}$$

Rearrangement of Eq. (7) leads to:

$$[^{\bullet}OH] = \frac{k_1 v_0 \lambda m t}{1 + k_1 v_0 \lambda t}. \tag{8}$$

The degradation of DNOC will be:

$$-\frac{d[\mathrm{DNOC}]}{dt} = k[{}^{\bullet}\mathrm{OH}][\mathrm{DNOC}] = kk_1\lambda v_0 mt\frac{[\mathrm{DNOC}]}{1+k_1v_0\lambda t} = \frac{[\mathrm{DNOC}]}{a+bt}t, \tag{9}$$

where $k$ is the pseudo second-order reaction rate constant ($\mu g^{-1}\,mL\,min^{-1}$) for this reaction and $a = 1/(kk_1\lambda v_0 m)$, $b = 1/(km)$ (min).

Integration of Eq. (9) leads to:

$$\ln\frac{[\mathrm{DNOC}]_t}{[\mathrm{DNOC}]_0} = -\frac{a}{b^2}\ln\left(\frac{a}{a+bt}\right) - \frac{t}{b}, \tag{10}$$

Eq. (9) has the same format as the modified Fenton model [36]:

$$-\frac{d[\mathrm{D}]}{dt} = kk_1\lambda\pi\omega v_0^2 t\frac{[\mathrm{D}]}{1+K_{\mathrm{D-Fe^{3+}}}\eta v_0 t} = \frac{[\mathrm{D}]}{a+bt}t, \tag{11}$$

where $a = 1/(kk_1\lambda\pi\omega v_0^2)$ and $b = K_{\mathrm{D-Fe^{3+}}}\eta/(kk_1\lambda\pi\omega v_0)$.

The model fitting results are shown in Fig. 7 and are found to match the experimental data very well for pH 2.8 ($R^2 = 0.9893$). The good fit of the model indicates that the mechanism proposed is a reasonable description of degradation in solution at pH 2.8. In this current experiment condition (pH = 2.8, initial concentration of $Fe^{2+}$ $m = 4.14\,\mu g\,mL^{-1}$, $[\mathrm{DNOC}]_0 = 11.4\,\mu g\,mL^{-1}$), the pseudo second-order reaction rate constant for DNOC degradation $k$ is measured as $1.79\times10^{-2}\,\mu g^{-1}\,mL\,min^{-1}$. The observed rate of DNOC degradation appears to be related to DNOC concentration and reaction time and can be expressed as:

$$-\frac{d[\mathrm{DNOC}]}{dt} = \frac{[\mathrm{DNOC}]}{13.16+13.47t}t. \tag{12}$$

Since there were other reactions contributing to the degradation of DNOC at neutral pH, this model does not apply to the neutral pH condition.

## 4. Conclusions

In conclusion, DNOC was successfully removed using nano-magnetite as the iron source and cathodic Fenton generation of hydrogen peroxide. At a near neutral pH (5.9), the degradation of DNOC is mainly due to direct electrolysis of the target compound on the electrode, and a heterogeneous reaction on the surface of the nano-magnetite is not obvious and does not contribute to the degradation of the target compound. The reaction at acidic pH (2.8) was mainly a homogeneous Fenton reaction in solution due to iron leaching from the oxide surface. Thus, nano-magnetite provides a steady iron source for the Fenton reaction. Under our experimental conditions, the use of chelating agents had no significant effect on DNOC degradation.

The degradation mechanism was described by a new model which was found to match the experimental data very well. Combined with nano-magnetite, cathodic Fenton was shown to effectively degrade the target compound under acidic pH conditions. However, this system degrades only half the target compound in 1 h at near neutral pH, primarily due to the dominance of direct electrolysis under this condition. To completely degrade the target compound, either an acidic condition or enough time is required to accomplish the task. The process for pesticide remediation that combines stable and reusable nano-magnetite with cathodically generated $H_2O_2$ can successfully simplify waste treatment, increase the efficiency and reduce treatment costs compared to less stable minerals. The large surface area of nano-magnetite enhances dissolution of iron at lower pH and thus the rate of degradation. Future work will explore the use of different kinds of nano-magnetite with different surface properties for a fast and efficient heterogeneous reaction at near neutral pH. The degradation of ionizable compounds with a strong adsorption affinity toward nano-magnetite will also be investigated. These approaches are environmentally sustainable and efficient.

## Acknowledgments

The study was funded in part by the College of Human Ecology, Cornell University and in part by the Cornell University Agricultural Experiment Station federal formula funds, Project No. NYC-329806 (W-1045), received from the Cooperative State Research, Education, and Extension Service, U.S. Department of Agriculture. Any opinions, findings, conclusions, or recommendations expressed in this publication are those of the author(s) and do not necessarily reflect the views of the U.S. Department of Agriculture.

## Appendix A. Supplementary data

Supplementary data associated with this article can be found, in the online version, at doi:10.1016/j.molcata.2011.03.001.

## References

[1] W.Z. Tang, C.P. Huang, Environ. Technol. 17 (1996) 1371–1378.
[2] S.-F. Kang, T.-H. Wang, Y.-H. Lin, J. Environ. Sci. Health, Part A: Toxic/Hazard. Subst. Environ. Eng. A 34 (1999) 935–950.
[3] L. Szpyrkowicz, C. Juzzolino, S.N. Kaul, Water Res. 35 (2001) 2129–2136.
[4] M.-J. Liou, M.-C. Lu, J. Mol. Catal. A: Chem. 277 (2007) 155–163.
[5] D.A. Saltmiras, A.T. Lemley, J. Agric. Food Chem. 48 (2000) 6149–6157.
[6] Q. Wang, A.T. Lemley, Environ. Sci. Technol. 35 (2001) 4509–4514.
[7] H. Liu, C. Wang, X. Li, X. Xuan, C. Jiang, H.n. Cui, Environ. Sci. Technol. 41 (2007) 2937–2942.
[8] M.A. Oturan, J. Peiroten, P. Chartrin, A.J. Acher, Environ. Sci. Technol. 34 (2000) 3474–3479.
[9] N. Oturan, M.A. Oturan, Agron. Sustain. Dev. 25 (2005) 267–270.
[10] I. Sires, C. Arias, P.L. Cabot, F. Centellas, J.A. Garrido, R.M. Rodriguez, E. Brillas, Chemosphere 66 (2007) 1660–1669.
[11] I. Sires, E. Guivarch, N. Oturan, M.A. Oturan, Chemosphere 72 (2008) 592–600.
[12] A. Wang, J. Qu, J. Ru, H. Liu, J. Ge, Dyes Pigments 65 (2005) 227–233.
[13] E. Brillas, I. Sires, M.A. Oturan, Chem. Rev. (Washington, DC, US) 109 (2009) 6570–6631.
[14] W.P. Kwan, B.M. Voelker, Environ. Sci. Technol. 37 (2003) 1150–1158.
[15] K. Hanna, T. Kone, G. Medjahdi, Catal. Commun. 9 (2008) 955–959.
[16] X. Xue, K. Hanna, N. Deng, J. Hazard. Mater. 166 (2009) 407–414.
[17] X. Xue, K. Hanna, C. Despas, F. Wu, N. Deng, J. Mol. Catal. A: Chem. 311 (2009) 29–35.
[18] X. Xue, K. Hanna, M. Abdelmoula, N. Deng, Appl. Catal. B 89 (2009) 432–440.
[19] E. Exposito, C.M. Sanchez-Sanchez, V. Montiel, J. Electrochem. Soc. 154 (2007) E116–E122.
[20] D.M. Whitacre, G.W. Ware, The Pesticide Book, 6th ed., MeisterPro Information Resources (Meister MediaWorldwide), Willoughby, OH, 2004.
[21] E. Halfon, R. Bruggemann, Water Sci. Technol. 21 (1989) 815–820.
[22] M Uebori, K. Imamura, Y. Hattori, H. Bandow, Mizu Kankyo Gakkaishi 31 (2008) 313–317.
[23] M.A. Oturan, I. Sires, N. Oturan, S. Perocheau, J.-L. Laborde, S. Trevin, J. Electroanal. Chem. 624 (2008) 329–332.
[24] C. Kormann, D.W. Bahnemann, M.R. Hoffmann, Environ. Sci. Technol. 22 (1988) 798–806.
[25] M.A.H. Franson, A.E. Greenberg, A.D. Eaton, L.S. Clesceri (Eds.), Standard Methods for the Examination of Water and Wastewater, 20th ed., American Public Health Association, 1998.
[26] U. Schwertmann, R.M. Cornell, Iron Oxides in the Laboratory: Preparation and Characterization, VCH, Weinheim, 1991, Fed. Rep. Ger.
[27] K. Hanna, J. Colloids Interface Sci. 309 (2007) 419–428.
[28] C. Flox, J.A. Garrido, R.M. Rodriguez, F. Centellas, P.-L. Cabot, C. Arias, E. Brillas, Electrochim. Acta 50 (2005) 3685–3692.
[29] K. Hanna, C. Carteret, Chemosphere 70 (2007) 178–186.
[30] A. Goi, M. Trapido, Chemosphere 46 (2002) 913–922.
[31] A. Dhaouadi, L. Monser, N. Adhoum, Electrochim. Acta 54 (2009) 4473–4480.
[32] K. Sehested, N. Getoff, F. Schwoerer, V.M. Markovic, S.O. Nielsen, J. Phys. Chem. 75 (1971) 749–755.
[33] T. Zhou, Y. Li, F.-S. Wong, X. Lu, Ultrason. Sonochem. 15 (2008) 782–790.
[34] V.N. Kosyakov, I.E. Veleshko, N.G. Yakovlev, L.F. Gorovoy, in: RRC "Kurchatov Institute", Moscow, Russia, 2003, pp. 188–204.
[35] P.K. Wattal, D.S. Deshingkar, C. Srinivas, D.B. Naik, S. Manohar, in: Bhabha Atomic Research Centre, Mumbai, India, 2003, pp. 121–136.
[36] Q. Wang, E.M. Scherer, A.T. Lemley, Environ. Sci. Technol. 38 (2004) 1221–1227.